Supporting Information

Schlosser et al. 10.1073/pnas.1318670111

SI Materials and Methods

Observations. Samples were collected during a cruise in the Atlantic Ocean in February–March 2011 on-board RRS *Discovery* (D361), conducted as part of the UK GEOTRACES program and during an Atlantic Meridional Transect (AMT; www.amt-uk.org) cruise (AMT-17) as described previously (1).

Water Sampling and First Treatment. Surface seawater was pumped into the trace-metal-clean laboratory using a Teflon diaphragm pump connected by acid-washed braided PVC tubing to a towed "fish" positioned at 3–4 m water depth. Samples were filtered in-line through 0.8/0.2-μm cartridge filter (AcroPak1000) into acid-washed low-density polyethylene bottles. Unfiltered seawater for dissolved inorganic P (DIP) analysis was dispensed into acid-cleaned, aged, high-density polyethylene bottles using clean-sample-handling techniques according to the Global Ocean Ship-based Hydrographic Investigations Program (GO-SHIP) nutrient protocols (2). The trace-metal samples were acidified with concentrated ultrapurity hydrochloric acid (HCl, Romil, UpA) to pH 1.9 (0.013 M H^+). The acidified samples were allowed to equilibrate for at least 24 h prior analysis of dissolved Fe (DFe) and dissolved Al (DAl).

Dissolved Iron Measurements. Dissolved Fe was determined using an in-line flow injection with chemiluminescence detection (3–5). The acidified samples (pH 1.9) were spiked with superpurity hydrogen peroxide (H_2O_2, Romil, SpA), allowed to equilibrate for at least 30 min, and then loaded onto a chelating iminodiacetic resin (Toyopearl AF-Chelate 650M). The resin was briefly rinsed with 18.2 MΩ cm ultra high purity water (UHP water) and then eluted with a 0.44 M HCl solution (Romil, SpA). The eluate was then injected into a reaction stream composed of 0.86 M ammonia, 0.29 M H_2O_2 (both Romil, SpA), and 0.3 mM luminol + 0.7 mM triethylenetetramine solution (both from Sigma-Aldrich) maintained at constant temperature at 39 °C and then passed into a Hamamatsu (HC135) photo counter. DFe concentrations were quantified using the method of standard addition made daily in acidified low-iron seawater (Atlantic Ocean surface water). Each sample was run in triplicate.

The analytical blank was determined daily and showed that the acid reagent blank (HCl and H_2O_2) was negligible, while the manifold blank did not exceed 0.06 nmol L^{-1}. The detection limit of this method was 0.06 nmol L^{-1} (defined as three times the SD of the system blank $n = 3$). The accuracy of the system was assessed daily by the determination of DFe in surface water SAFe S and deep water D2 collected during the Sampling and Analysis of Fe (SAFe) program and in GEOTRACES surface (GS) and deep (GD) seawater reference materials. The concentration of DFe measured during this study was SAFe S = 0.095 ± 0.011 nmol L^{-1} ($n = 5$), SAFe D2 = 0.933 ± 0.035 nmol L^{-1} ($n = 5$), GEOTRACES GD = 0.940 ± 0.056 nmol L^{-1} ($n = 6$), and GS = 0.424 ± 0.026 nmol L^{-1} ($n = 5$). The surface GEOTRACES standard measurements were somewhat lower than the reported consensus value of 0.561 nmol L^{-1}, but all other standard seawater were in good agreement (GD = 1.03 nmol L^{-1}; SAFe S = 0.096 nmol L^{-1}; SAFe D2 = 0.958 nmol L^{-1}).

Dissolved Aluminum Measurements. Dissolved Al concentrations were analyzed using flow injection with lumogallion-Al fluorescence technique originally developed by Resing and Measures (6) and adapted to modifications published in Brown and Bruland (7). Acidified seawater samples were buffered before analysis to pH 5.2 ± 0.1 with ultraclean 2 M ammonium acetate buffer (Romil, UpA). The buffered sample was preconcentrated onto the Toyopearl resin and subsequently rinsed with UHP water. The retained Al was eluted from the column with 0.1 M HCl UpA and entered the reaction stream, where it mixed with a 58 μM lumogallion (MP Biomedicals) solution containing 2 M ammonium acetate buffer (pH 9.0) (Romil, UpA) and heated to 60 °C using a water bath. The eluent was then mixed with the 2.5% Brij-35 solution in another mixing coil. The emission of the fluorescent complex was detected by a Shimadzu RF-10A XL fluorometer, with excitation and emission wavelength set to 484 and 552 nm, respectively.

Each sample was run in duplicate and DAl concentrations were quantified using the method of standard additions made daily in acidified low-Al seawater (Atlantic Ocean deep water). The analytical blank was determined daily and the acid reagent blank determined running an unbuffered acidified seawater sample and a double buffered seawater sample, respectively was negligible ~0.04 nmol L^{-1}, and the manifold blank was ~0.9 nmol L^{-1}. The detection limit of the method was 0.25 nmol L^{-1}. For further quality control, subsamples of individual 500 mL seawater samples were measured daily and the average concentration was 9.7 ± 1.5 nmol L^{-1} ($n = 21$).

N_2 Fixation Measurements and Trichodesmium Abundances. Rates of N_2 fixation and *Trichodesmium* spp. abundance during the 2011 cruise were measured using identical methods to those previously described for AMT-17 (1). Water samples for N_2-fixation measurements were collected at five depths in the upper water column, spanning the region between the surface and the deep chlorophyll maximum. N_2 fixation was measured using the $^{15}N_2$ technique (8) following similar procedures to those described elsewhere (9, 10). In brief, samples were collected into 4.5 L acid-washed polycarbonate bottles, filled to the top, and then sealed without bubbles using a Teflon-lined septum. Following the addition of 4 mL $^{15}N_2$ gas (99% CK gasses), samples were incubated for 24 h on deck, with bottles screened to approximate in situ light levels. Incubations were terminated by gentle filtration onto precombusted GF/F filters (Whatman). Recent work suggests that this bubble injection method systematically underestimates the actual N_2 fixation rates due to incomplete and progressive equilibration of the gas and dissolved phase $^{15}N_2$ during the incubation (11, 12). In the context of the current study we note that none of our conclusions will be sensitive to the absolute rates of N_2 fixation occurring in the region and hence the likely ~twofold systematic underestimation of the technique used (11–13) has no bearing. Moreover, even assuming the extreme and variable underestimation (~16–100%), which has been reported in some cases (11, 13), this would not be sufficient to qualitatively alter the observed gradients between regions of low and enhanced N_2 fixation in the current study, where measured rates spanned >2 orders of magnitude (Fig. S6).

Samples for *Trichodesmium* spp. abundance were prepared by gentle filtration of 20 L of surface water onto a Millipore Isopore 47 mm, 10-μm pore size filter followed by resuspension into 100-mL filtered seawater and preservation in 2% Lugol's iodine solution. Colonies and free filaments were enumerated by light microscopy on return to shore (1, 14).

Numerical Modeling. To further illustrate and explore the system dynamics we expanded a previously used simple numerical box

model (15–17). The model simulates the interactions between two broad planktonic groups of phytoplankton and diazotrophs in competition for three nutrients (N, P, and Fe). The model was extended to include an idealized representation of a surface and deep/thermocline layer by linking together boxes in series, with an imposed exchange rate between sequential boxes (k) (Fig. S5). The differential equations describing the evolution of the state variables within the surface box were effectively identical to those used by Ward et al. (17), and the deep/thermocline box simply acts as a nutrient reservoir and remineralization region. Thus, a surface box is supplied with nutrients from the immediate proceeding deep box, with a fraction of the standing stock of biological material (phyt + diaz) formed in the surface box being mixed/diluted out into the subsequent deep box, where it is immediately remineralized back to the inorganic nutrient pool and can hence act as the reservoir for the subsequent surface box etc. Similar to the previous study of Ward et al. (17), the only external forcing provided to the model is then a variable source of DFe to the surface boxes, here assumed to represent an idealized atmospheric Fe input. Parameters and initial conditions are presented in Table S1. The corresponding full set of model equations are:

Nutrient limitation terms

$$\gamma_{phyt} = \min\left[\frac{N}{k_{phyt,N}+N}, \frac{P}{k_{phyt,P}+P}, \frac{Fe}{k_{phyt,Fe}+Fe}\right]$$

$$\gamma_{diaz} = \min\left[\frac{P}{k_{diaz,P}+P}, \frac{Fe}{k_{diaz,Fe}+Fe}\right]$$

Time rate of change of state variables

$$\frac{dphyt_j}{dt} = \mu_{max,phyt}\ \gamma_{phyt}\ phyt_j - m_{phyt}\ phyt_j - k\ phyt_j$$

$$\frac{ddiaz_j}{dt} = \mu_{max,diaz}\ \gamma_{diaz}\ diaz_j - m_{diaz}\ diaz_j - k\ diaz_j$$

$$\frac{dN_j}{dt} = -\mu_{max,phyt}\ \gamma_{phyt}\ phyt_j - \mu_{max,diaz}\ \gamma_{diaz}\ diaz_j + m_{phyt}\ phyt_j + m_{diaz}\ diaz_j + k\left(DeepP_j - P_j\right)$$

$$\frac{dP_j}{dt} = -\mu_{max,phyt}\ \gamma_{phyt}\ phyt_j/R_{NP} - \mu_{max,diaz}\ \gamma_{diaz}\ diaz_j/R_{NP} + m_{phyt}\ phyt_j/R_{NP} + m_{diaz}\ diaz_j/R_{NP} + k\left(DeepN_j - N_j\right)$$

$$\frac{dFe_j}{dt} = -\mu_{max,phyt}\gamma_{phyt}\ phyt_j/R_{NFe,phyt} - \mu_{max,diaz}\ \gamma_{diaz}\ diaz_j/R_{NFe,diaz} + m_{phyt}\ phyt_j/R_{NFe,phyt} + m_{diaz}\ diaz_j/R_{Nfe,diaz} + k\left(DeepFe_j - Fe_j\right) + Fe_{atm,j}$$

$$\frac{dDeepN_{j+1}}{dt} = -k\left(DeepN_{j+1} - N_j\right) + k\left(phyt_j + diaz_j\right)$$

$$\frac{dDeepP_{j+1}}{dt} = -k\left(DeepP_{j+1} - P_j\right) + k\left(phyt_j + diaz_j\right)/R_{NP}$$

$$\frac{dDeepFe_{j+1}}{dt} = -k\left(DeepFe_{j+1} - Fe_j\right) + k\left(phyt_j/R_{NFe,phyt} + diaz_j/R_{NFe,diaz}\right) - scav$$

Nonstandard parameter ranges in parenthesis.

With a time-invariant external forcing, the set of linked surface and deep boxes can actually be thought of as representing two scenarios. Conceptually, the system can be assumed to represent the time evolution of feedbacks within a static water column composed of surface and thermocline waters, with the variable surface Fe input thus representing some temporal change. In contrast, in the current context, rather than representing a fixed location, we conceptually interpret the steady-state solution of the system as representing feedbacks between surface and thermocline waters along a large-scale circulation path from the southern to northern subtropical gyres of the Atlantic Ocean within the upper limb of the overturning circulation (1, 18). Note that these two interpretations of a steady-state solution are effectively equivalent, with the second representing an idealized Lagrangian description of a water parcel as it moves slowly northwards within the upper ocean meridional circulation rather than remaining at a fixed location. Moreover, with adopted configuration, the ratio of biological mortality and hence remineralization in the surface box, to mixing/dilution out of the surface box, defines the efficiency of recycling within the surface layer and hence equivalently the ratio of exported organic production to total production (ef ratio) (19). By varying the parameters that dictate the effective ef ratio we can thus consider whether the model is sensitive to processes that could similarly alter the actual ef ratio in the real system, including, for example, changes in vertical mixing/upwelling within different regions or variable efficiencies of particulate matter export for different communities.

Provided the model is initialized with an excess of DIP relative to dissolved inorganic nitrogen (DIN) in the deep box (17), despite quantitative differences, which can be readily reconciled with the well-developed theory (16, 17), the characteristic behavior that emerges from steady-state solutions is largely insensitive to parameter choices, variability in the form of the imposed surface Fe input, and any assumption concerning loss of Fe to scavenging processes (Fig. S4). Consequently, the model fully supports our suggested role of reciprocal feedbacks between Fe, P, and diazotrophy in setting the large-scale biogeochemical division of the Atlantic (1, 20).

When forcing the model with a time-varying surface Fe input as an idealized representation of the seasonal migration of the ITCZ, the model retains a similar qualitative lack of sensitivity to Fe scavenging; however, the differences in quantitative behavior including, for example patterns of diazotrophy, become more apparent, particularly in relation to alterations in parameters that can influence the effective ef ratio (Fig. S5). Under the non-steady-state configuration, we interpret these differences as representing the ability of the biogeochemical feedbacks within the model to keep pace with the time-varying external forcing. However, despite this sensitivity, the model still behaves in a robust characteristic manner, with the region of diazotrophy tracking movements in the region of maximal surface Fe input, alongside the boundary between, for example, the high- and low-P waters, albeit to a variable degree (Fig. 3 and Fig. S5). As a consequence, despite the lack of any real physical forcing within the model, the robustness of the characteristic behavior to variations in effective ef ratio and hence equivalently differences in the importance of vertical nutrient supply to surface recycling thus suggest the first-order sensitivity of the system to alterations in surface Fe inputs would not be sensitive to a more realistic complex three-dimensional circulation.

1. Moore CM, et al. (2009) Large-scale distribution of Atlantic nitrogen fixation controlled by iron availability. *Nat Geosci* 2(12):867–871.
2. Hydes DJ, et al. (2010) Detrmination of dissolved nutrients (N, P, Si) in seawater with high precision and inter-comparability using gas-segment continuous flow analyzer. *GO-Ship Repeat Hydrography Manual: A Collection of Expert Reports and Guidelines,* IOCCP Rep No 14, ICPO Publication Series No 134, Version 1.
3. Obata H, Karatani H, Nakayama E (1993) Automated determination of iron in seawater by chelating resin concentration and chemiluminescence detection. *Anal Chem* 65:1524–1528.
4. de Jong JTM, et al. (1998) Dissolved iron at subnanomolar levels in the Southern Ocean as determined by ship-board analysis. *Anal Chim Acta* 377(2-3):113–124.
5. Klunder MB, Laan P, Middag R, De Baar HJW, Ooijen Jv (2011) Dissolved iron in the Southern Ocean (Atlantic sector). *Deep Sea Res Part II Top Stud Oceanogr* 58(25-26): 2678–2694.
6. Resing JA, Measures CI (1994) Fluorometric determination of Al in seawater by flow injection analysis with in-line preconcentration. *Anal Chem* 66(22):4105–4111.
7. Brown MT, Bruland KW (2008) An improved flow-injection analysis method for the determination of dissolved aluminum in seawater. *Limnol Oceanogr Methods* 6:87–95.
8. Montoya JP, Voss M, Kahler P, Capone DG (1996) A simple, high-precision, high-sensitivity tracer assay for N_2 fixation. *Appl Environ Microbiol* 62(3):986–993.
9. Mills MM, Ridame C, Davey M, La Roche J, Geider RJ (2004) Iron and phosphorus co-limit nitrogen fixation in the eastern tropical North Atlantic. *Nature* 429(6989): 292–294.
10. Voss M, Croot P, Lochte K, Mills M, Peeken I (2004) Patterns of nitrogen fixation along 10°N in the tropical Atlantic. *Geophys Res Lett* 31(23):L23S09.
11. Großkopf T, et al. (2012) Doubling of marine dinitrogen-fixation rates based on direct measurements. *Nature* 488(7411):361–364.
12. Mohr W, Grosskopf T, Wallace DWR, LaRoche J (2010) Methodological underestimation of oceanic nitrogen fixation rates. *PLoS ONE* 5(9):e12583.
13. Wilson ST, Böttjer D, Church MJ, Karl DM (2012) Comparative assessment of nitrogen fixation methodologies, conducted in the oligotrophic North Pacific Ocean. *Appl Environ Microbiol* 78(18):6516–6523.
14. Tyrrell T, et al. (2003) Large-scale latitudinal distribution of *Trichodesmium* spp. in the Atlantic Ocean. *J Plankton Res* 25(4):405–416.
15. Tyrrell T (1999) The relative influences of nitrogen and phosphorus on oceanic primary production. *Nature* 400:525–531.
16. Dutkiewicz S, Ward BA, Monteiro F, Follows MJ (2012) Interconnection of nitrogen fixers and iron in the Pacific Ocean: Theory and numerical simulations. *Global Biogeochem Cycles* 26(1):1–16.
17. Ward BA, Dutkiewicz S, Moore CM, Follows MJ (2013) Iron, phosphorus and nitrogen supply ratios define the biogeography of nitrogen fixation. *Limnol Oceanogr* 58(6): 2059–2075.
18. Palter JB, Lozier MS, Sarmiento JL, Williams RG (2011) The supply of excess phosphate across the Gulf Stream and the maintenance of subtropical nitrogen fixation. *Global Biogeochem Cycles* 25(4):1–14.
19. Laws EA, Falkowski PG, Smith WO, Ducklow H, McCarthy JJ (2000) Temperature effects on export production in the open ocean. *Global Biogeochem Cycles* 14(4):1231–1246.
20. Wu J, Sunda W, Boyle EA, Karl DM (2000) Phosphate depletion in the western North Atlantic Ocean. *Science* 289(5480):759–762.

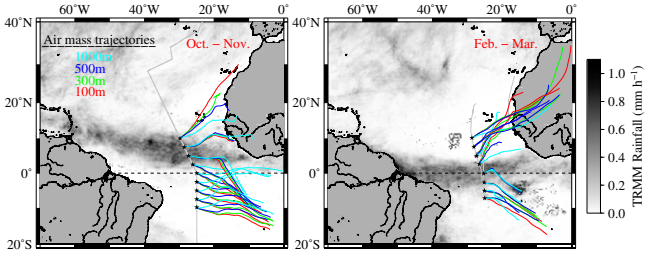

Fig. S1. Airmass trajectories, over the 4 d before occupation using the Hybrid Single-Particle Lagrangian Integrated Trajectory algorithm, at 100 m (red), 300 m (green), 500 m (dark blue), and 1,000 m (sky blue) at certain points in the tropical Atlantic Ocean along the cruise track of AMT-17 (*Left*) and D361 (*Right*). Satellite rainfall rates (Tropical Rainfall Measuring Mission) of AMT-17 and D361 are illustrated by different shades of gray.

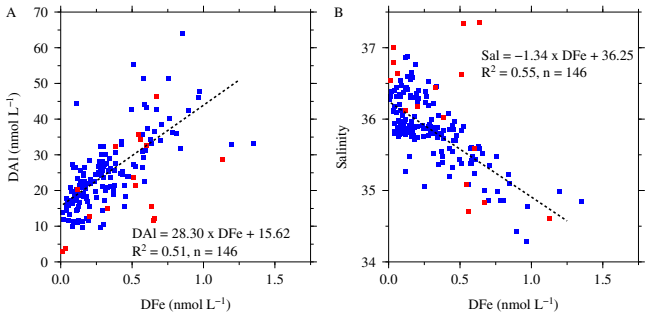

Fig. S2. *A* illustrates the linear relationship of DFe and DAl for samples collected during D361 (blue) and AMT-17 (red). *B* shows the relationship of DFe and Salinity for the same samples. The relationship of the D361 and the AMT-17 data set looks remarkably similar, despite the spatial offset.

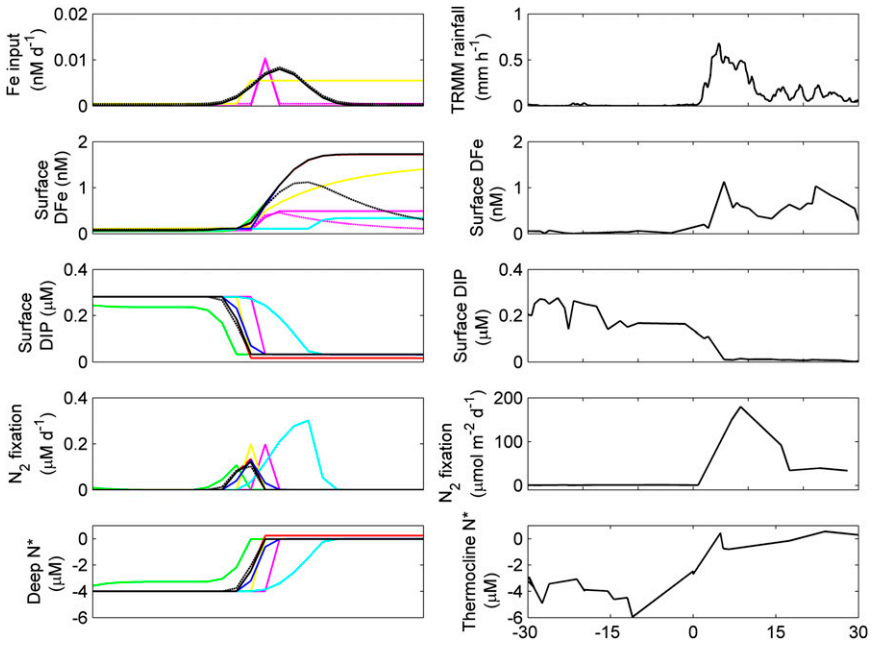

Fig. S3. Steady-state model implementations over a range of parameter values and modeled Fe input and scavenging functions (*Left*) compared with data from the AMT-17 cruise (*Right*). General model behavior is robust to the wide variety of parameter choices and model forcings implemented, with the characteristic pattern of HPLFe and LPHFe waters being delineated by the region of enhanced diazotrophy apparent in all cases and qualitative equivalent to observed latitudinal gradients in the Atlantic Ocean. Similarly, the excess of DIP (-ve N*, where N* = DIN − 16 × DIP), which is initially imposed in the subsurface "thermocline" boxes is removed downstream of the region of enhanced diazotrophy within the model, with the implication that the same process will be responsible for the zero or even +ve N* values observed in the subtropical North Atlantic thermocline. Dashed and solid lines indicate steady states with and without Fe scavenging respectively over a range of different Fe input functions (*Top Left*). All parameter values as in standard case (ef ratio = 0.1) (Table S1), except for: $\mu_{diazo} = 0.2$ (blue), $k_{Fe,diazo} = 0.05$, $R_{NFe,diazo} = 10$ (green), $k_P = 0.015$ (red), $m_{diaz} = 0.0125$, and $k = 0.25$ (ef ratio =0.5) (cyan).

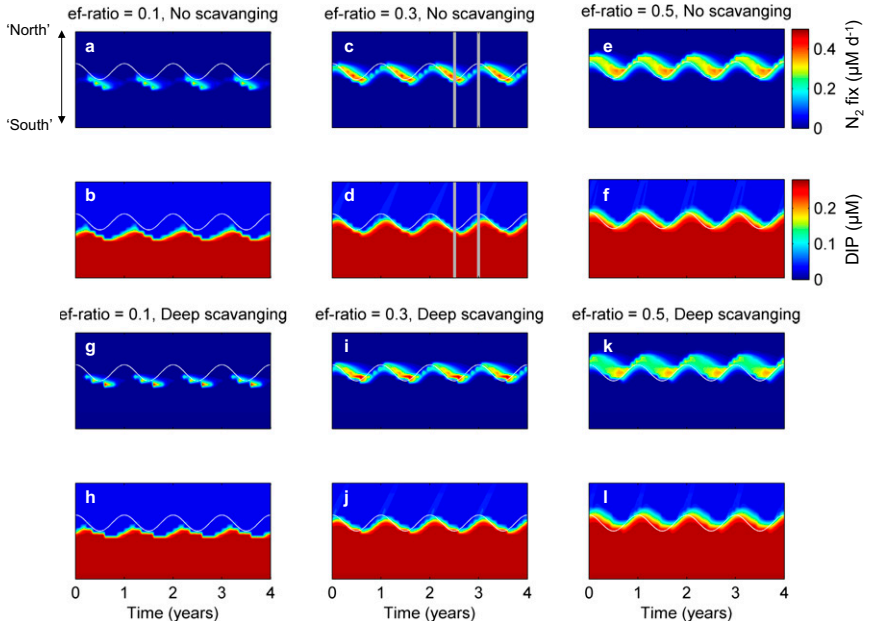

Fig. S4. Outputs from dynamic model runs time-varying position of maximum external Fe input, as indicated by the thin white line. Model implementations were performed with a range of different recycling efficiencies in the surface boxes and with and without implementation of deep water scavenging in the thermocline boxes. All parameters were the same as the standard case with the exception that the effective ef ratio was altered from 0.1 (*A, B, G,* and *H*) to 0.3 (*C, D, I,* and J) to 0.5 (*E, F, K,* and *L*), while scavenging was implemented in (*G–L*). Despite differences in details between model implementations, the qualitative behavior is consistent between runs and hence insensitive to parameterization. Specifically, modeled rates of near surface diazotrophy (*A, C, E, G, I,* and *K*) indicate that the region of enhanced rates tracks the seasonal movement of enhanced Fe inputs, with the location of the biogeochemical divide, as indicated by the boundary between high- and low-DIP waters (*B, D, F, H, J,* and *L*), moves "north" and "south" alongside movement of the location of maximal Fe input.

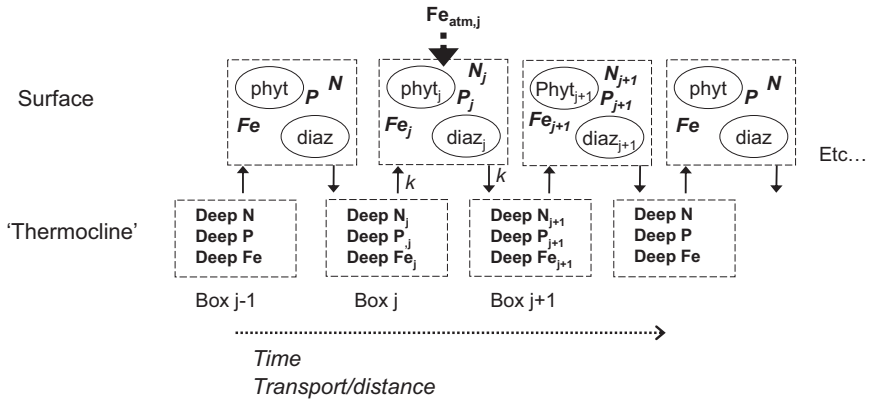

Fig. S5. Schematic description of model configuration, see Table S1 for variable descriptions, and *SI Materials and Methods* for equations and parameter descriptions.

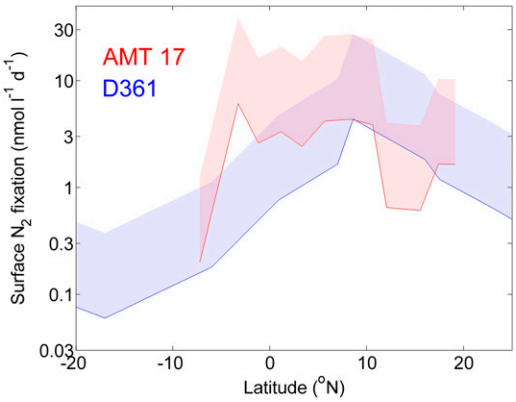

Fig. S6. Estimated range of potential sensitivity in observed N_2-fixation gradients to any methodological underestimation of rates (1, 2). Solid lines indicate measured near-surface N_2-fixation rates along two transects with shaded regions indicating the potential range of underestimation based on published studies. Note the logarithmic scale indicating the large gradients in N_2 fixation observed in the region. Also note that the gradient between the region of high-N_2 fixation around and north of the equator and the southward shift of the region of enhanced N_2 fixation between AMT-17 and D361 would both be robust to even extreme values and degree of variability in underestimation (11, 12).

Table S1. Variable names and starting conditions used in the idealized model

Symbol	Description	Units	Value(s)
phyt	Phytoplankton biomass	μM N	
diaz	Diazotroph biomass	μM N	
N	Surface DIN	μM N	
P	Surface DIP	μM P	
Fe	Surface DFe	nM Fe	
DeepN	Deep DIN	μM N	
DeepP	Deep DIP	μM P	
DeepFe	Deep DFe	nM Fe	
Fe_{atm}	Atmospheric DFe input	nM d^{-1}	Variable forcing
$DeepN_0$	Initial deep DIN	μM N	2
$DeepP_0$	Initial deep DIP	μM P	0.375
$DeepFe_0$	Initial deep DFe	nM Fe	0.1
$\mu_{max,phyt}$	Maximum phytoplankton growth rate	d^{-1}	1
$\mu_{max,diaz}$	Maximum diazotroph growth rate	d^{-1}	0.5 (0.2)
$R_{NFe,phyt}$	Phytoplankton N:Fe ratio	mol:mmol	50
$R_{NFe,diaz}$	Diazotroph N:Fe ratio	mol:mmol	5 (10)
R_{NP}	Phytoplankton N:P ratio	mol:mol	16
$K_{phyt,N}$	Phytoplankton DIN half-saturation constant	μM N	0.5
$K_{phyt,P}$	Phytoplankton DIP half-saturation constant	μM P	0.03 (0.015)
$K_{diaz,P}$	Diazotroph DIP half-saturation constant	μM P	0.03 (0.015)
$K_{phyt,Fe}$	Phytoplankton DFe half-saturation constant	nM Fe	0.01
$K_{diaz,Fe}$	Diazotroph DFe half-saturation constant	nM Fe	0.1 (0.05)
m_{phyt}	Phytoplankton mortality	d^{-1}	0.45 (0.3)
m_{diaz}	Diazotroph mortality	d^{-1}	0.2125 (0.0125)
k	Mixing/dilution rate	d^{-1}	0.05 (0.25)
scav	Deep DFe scavenging rate	d^{-1}	0 (0.01)
	Effective ef ratio (mortality/dilution)		0.1–0.5

Variable names and starting conditions used in the idealized model. Nonstandard parameter ranges in parentheses.